Journal of Solid State Chemistry 181 (2008) 1678–1683

Contents lists available at ScienceDirect

Journal of Solid State Chemistry

journal homepage: www.elsevier.com/locate/jssc

$K_4Nb_6O_{17}$-derived photocatalysts for hydrogen evolution from water: Nanoscrolls versus nanosheets

Michael C. Sarahan [a,b], Elizabeth C. Carroll [a], Mark Allen [a], Delmar S. Larsen [a], Nigel D. Browning [b,c], Frank E. Osterloh [a,*]

[a] Chemistry Department, University of California, One Shields Avenue, Davis, CA 95616, USA
[b] Chemistry and Materials Science Department, University of California, One Shields Avenue, Davis, CA 95616, USA
[c] Lawrence Livermore National Laboratory, 7000 East Avenue, Livermore, CA 94550, USA

ARTICLE INFO

Article history:
Received 17 April 2008
Received in revised form
6 June 2008
Accepted 10 June 2008
Available online 14 June 2008

Keywords:
Nanosheets
Nanoscrolls
Exfoliation
Photocatalysis
Water splitting
Hydrogen

ABSTRACT

The layered hexaniobate $K_4Nb_6O_{17}$ is known as a photocatalyst for methanol dehydrogenation and hydrogen evolution from water under ultraviolet (UV) light. Here we show that the activity is retained in propylammonium- (PA) or tetrabutylammonium- (TBA) stabilized $H_2K_2Nb_6O_{17}$ nanosheets and TBA-stabilized $H_4Nb_6O_{17}$ nanoscrolls that can be obtained by exfoliation of $K_4Nb_6O_{17}$ followed by cation exchange. The catalytic activity of the exfoliated systems is comparable to $K_4Nb_6O_{17}$, with scrolls being most active in water, and PA sheets giving enhanced H_2 rates due to sacrificial electron donor action of PA. Femtosecond absorption spectra for TBA scrolls and PA sheets exhibit broad features between 450 and 700 nm due to trapped holes and electrons. Electron–hole recombination follows approximately second-order kinetics, with rates of decay similar for sheets and scrolls. In addition, catalysts were characterized with UV/vis and fluorescence spectroscopy and transmission electron microscopy.

1. Introduction

The hexaniobate $K_4Nb_6O_{17}$ has been known for over 20 years as an active catalyst for methanol dehydrogenation under ultraviolet (UV) irradiation [1]. From water the catalyst evolves hydrogen at low rates and oxygen at sub-stoichiometric rates, but stoichiometric H_2/O_2 evolution with quantum efficiencies of 5.3–20% is possible after modification with 0.1 wt% NiO [2–5] or after internal platinization [6]. The structure of $K_4Nb_6O_{17}$ consists of stacked asymmetrical $Nb_6O_{17}^{4-}$ layers (Fig. 1), which are composed of edge- and corner-shared NbO_6 octahedra. Depending on layer orientation, stacking produces two kinds of potassium-filled interlayers, denoted as I and II [7]. It has been hypothesized that water reduction occurs in interlayer I and water oxidation at interlayer II, and that an electric field gradient originating from the uneven K^+ ion distribution on both sides of the sheets may assist in electron–hole separation [6,8]. To shed further light onto the photocatalytic mechanism and the location of the active sites, and to determine whether the layer interaction is a requirement for the photocatalytic properties of $K_4Nb_6O_{17}$, we have performed photochemical studies on exfoliated niobate layers in water and in aqueous methanol. Nanosheets that contain double niobate layers can be obtained as individual nanoparticles by reaction of $K_4Nb_6O_{17}$ with propylammonium (PA) hydrochloride [9]. Reaction with HNO_3, on the other hand, followed by treatment with tetrabutylammonium (TBA) hydroxide produces TBA nanoscrolls, which contain niobate layers folded onto themselves [10]. Due to the folding, these nanoscrolls produce a new type of interlayer III, not represented in the structure of $K_4Nb_6O_{17}$ (Fig. 1), whereas the nanosheets contain only interlayers of type II. As we will show here, both sheets and scrolls are effective catalysts for H_2 evolution from water and aqueous methanol, with overall activities modulated by the morphology and stacking of the nanosheets, and by the surfactants that stabilize them. Optical measurements suggest a reduced bandgap of the scrolls resulting from bending of the niobate layer, and femtosecond transient absorption measurements reveal differences in the excited state dynamics in the two systems that suggest scrolls support a greater number of trapped electrons than sheets.

2. Experimental

Optical measurements were performed in standard quartz cuvettes using a Jobin-Ivon *Fluoromax-P* fluorimeter. UV/vis spectra were collected using an Ocean Optics DH2000 light

* Corresponding author. Fax: +1 530 752 8995.
E-mail address: fosterloh@ucdavis.edu (F.E. Osterloh).

0022-4596/$ - see front matter © 2008 Elsevier Inc. All rights reserved.
doi:10.1016/j.jssc.2008.06.021

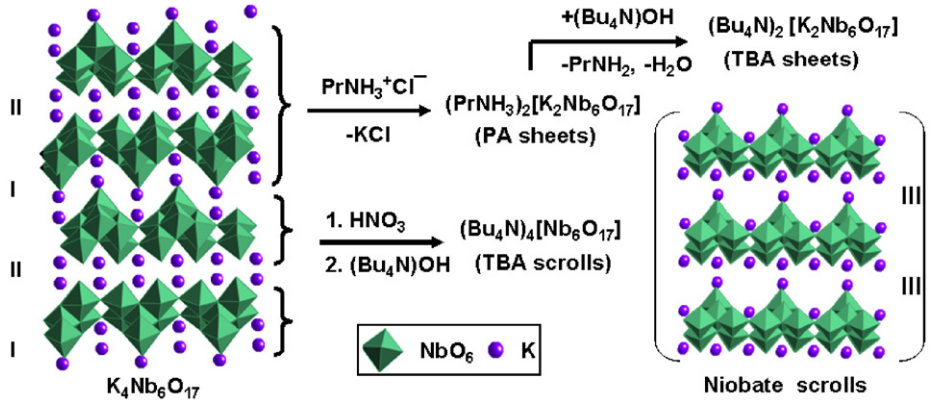

Fig. 1. Synthesis of niobate nanosheets and nanoscrolls. The structure of $K_4Nb_6O_{17}$ and the tentative structure of niobate nanoscrolls are also shown.

source and an HR2000 CG-UV-NIR spectrometer. A Fisher Scientific Marathon 21000 centrifuge at 13750 rpm was employed for centrifugation. Transmission electron micrographs were obtained on a Philips CM-12 instrument at 120 kV acceleration potential. Scanning transmission electron micrographs were obtained on a JEOL JEM2500SE instrument at 200 kV acceleration potential. Ultrasonication was performed for <5 min using a 90 W ultrasonic cleaner (Fisher Scientific, model FS 20).

2.1. Potassium niobates

Potassium hexaniobate, $K_4Nb_6O_{17}$, was obtained by heating a shaken and pulverized mixture of potassium carbonate (3.157 g, 30.57 mmol, Acros ACS Reagent grade) and niobium (V) oxide (8.127 g, 22.84 mmol, Acros 99.9% purity) for the stoichiometric 3:2 m ratio [11]. The mixture was formed into pellets in a pellet press with 6.5 metric tons of force. The pellets were calcined at 1100 °C for 48 h in alumina crucibles. The resulting yellowish crystalline material was pulverized into a fine white powder using mortar and pestle. The structure of the material was confirmed by X-ray powder diffraction with a Scintag XDS-2000 powder X-ray diffractometer with a copper *K*-α line-focus tube.

2.2. Propylammonium exfoliation

Propylamine hydrochloride was obtained from Acros as 99+% purity. In all, 2.00 g (1.93 mmol) of the potassium niobate product (with $3\times H_2O$) was stirred for 9 days with 3.88 g (40.60 mmol) propylamine hydrochloride in approximately 100 mL deionized (>18 MΩ cm resistivity) water in an oil bath at 80 °C. The resulting mixture was centrifuged at 13750 rpm for 10 min. The supernatant was poured off, and the solid was redistributed with sonication in approximately 20 mL pure water. Centrifugation and redistribution were repeated twice more, for a total of three washes. The final solid was redistributed in 50 mL pure water with shaking and sonication. The concentration of sheets in the solution was measured by evaporating the solvent from 1.00 mL of the sample and weighing the remaining residue. The concentration of sheets was measured to be 24.67 mg/mL, which corresponds to 1.234 g $K_2(PrNH_3)_2[Nb_6O_{17}]$ catalyst (62% yield, $M=1028$ g/mol).

2.3. Tetrabutylammonium hydroxide exfoliation

For the acid/TBA(OH) exfoliation, acid treatment of 2.0 g (1.93 mmol) potassium niobate trihydrate was carried out at room temperature for 5 days with 250 mL of 1.0 M (500× molar excess) sulfuric acid. The product was centrifuged after the fifth day, and washed with approximately 20 mL pure water three times. TBA hydroxide (40 wt% in water, Acros) was added to the wet solid in a 20:1 molar ratio (26.6 mL, 40.5 mmol). This mixture was stirred for 6 days, and the product was centrifuged and washed three times with approximately 20 mL water. 45 mL water was added to the precipitate, and the mix was shaken and sonicated until the solution was a homogeneous suspension. The concentration of sheets was measured to be 11 mg/mL, which corresponds to a total of 0.495 g $(Bu_4N)_4[Nb_6O_{17}]$ (14% yield, $M=1797$ g/mol). Losses are likely due to nanosheets remaining in the supernatant that is poured off after each wash. Later exfoliations were performed with longer centrifugation times during washing and attained higher yields. The scrolls have been observed in the supernatant visibly as white cloudiness in water, lacking the strong birefringence of the sheets. Observation of the supernatant and final redistributed sample by transmission electron microscopy (TEM) shows a thin rod-like structure, with edges showing the layers of the scrolls.

2.4. Tetrabutylammonium sulfate ion exchange

To prepare materials that differed only in morphology, and not in counterion, the PA exfoliated suspension was treated with ~5% TBA sulfate. This solution was prepared by neutralizing TBA hydroxide with sulfuric acid, to a final pH of approximately 7. Approximately 5 mL of the PA exfoliated suspension was stirred with 50 mL of the 5% TBA sulfate for 30 min. This solution was rinsed and centrifuged three times, and tested for primary amine content using the ninhydrin test (5 mg ninhydrin in 50 mL water, pH made basic using 1.0 M KOH). After three treatments, the suspension tested negative for primary amines.

2.5. Photolysis experiments

Photochemical hydrogen generation experiments were carried out at 30 °C using a quartz flask that was exposed to the light of four low-pressure 175 W mercury lamps. The photon flux in the glass flask was found to be $5.3\pm0.4\times10^{16}$ photons/s for the 250–500 nm spectral region of the lamps, as determined with ferrioxalate chemical actinometry. For catalytic measurements, the catalyst suspension (100 mg catalyst in 75 mL of water) was placed in a quartz flask. The flask was evacuated to 30 Torr and held there for 5 min. The flask was then filled with argon to atmospheric pressure and evacuated again. This was repeated for a total of 3 evacuation/fill cycles. An online gas chromatograph system consisting of a Varian 3800 gas chromatograph with a thermal conductivity detector was used to analyze the gas in the reaction apparatus. An initial measurement was made to verify

the absence of hydrogen, oxygen and nitrogen. The hydrogen content of the gas was checked periodically during exposure using the aforementioned sampling procedure.

2.6. Transient absorption

The early photodynamics of charge carriers were characterized using a dispersed transient absorption spectrometer, which has been described in detail previously [12]. Suspensions of either sheets or scrolls in water and aqueous methanol were excited with 300-nm, 200-fs pulses, and the photodynamics were monitored by the visible absorption of trapped charge carriers. Transient absorption experiments were also carried out on samples following 6 h irradiation in the Hg-lamp photolysis chamber.

3. Results and discussion

TEM and scanning TEM were used to confirm the morphology of scrolls and sheets (Fig. 2). Cation exchange with TBA does not affect the sheet morphology as long as the exchange is carried out at room temperature and for periods not exceeding 30 min. Prolonged reaction does convert sheets into scrolls (see Supporting information).

During photoirradiation about 10% of the TBA sheets convert into scrolls (see Fig. 2C), a process that may be facilitated by the slightly elevated temperature (30 °C) in the photoreactor. Scrolls obtained by reaction of $K_4Nb_6O_{17}$ with acid/TBA(OH) are shown in Fig. 2B. The morphology resembles that described in earlier reports [10]. Remarkably, the diameter of the scrolls lies within a very narrow range of 25 ± 6 nm, as measured on TEM and STEM images. UV irradiation over 6 h leaves the scroll morphology mostly intact. Some observed bends and partial unrolling could be caused by the stirring and mechanical forces during workup (Fig. 2D).

Diffuse reflectance UV–visible spectra and emission spectra of the hexaniobate, and the nanoscrolls and nanosheets are shown in Fig. 3 and selected optical data are summarized in Table 1. It can be seen that the absorption edges vary with the morphology of the materials, and are increasingly shifted towards the visible in the order $K_4Nb_6O_{17}$ < nanosheets < nanoscrolls. Exchanging the counterion PA with TBA in the nanosheets causes a blue shift of 8 nm that might be due to differences in nanosheet–surfactant interactions. Kudo and Sakata [13] have argued that protonation of the niobate converts surface Nb=O bonds into weaker Nb–OH bonds, reducing the bandgap of the material. Replacing the hydrogen bond donor PA with an aprotic counterion should then increase the double bond character of the Nb–O bond, increasing the bandgap and blue-shifting the absorption edge.

Based on absorption edges, bandgaps of the materials lie in the range of 3.44 (for PA sheets) to 3.56 eV (for $K_4Nb_6O_{17}$), which agrees with the literature value for $K_4Nb_6O_{17}$ [14]. For TBA scrolls the bandgap is reduced to 3.30 eV, possibly due to Nb–O–Nb bond weakening because of the bend of the niobate layers in the scrolls. When dispersed in water, all four materials also exhibit photoluminescence at room temperature under bandgap excitation. For $K_4Nb_6O_{17}$, the emission maximum is observed at 376 nm, which is blue-shifted from previous low temperature (77 K) measurements

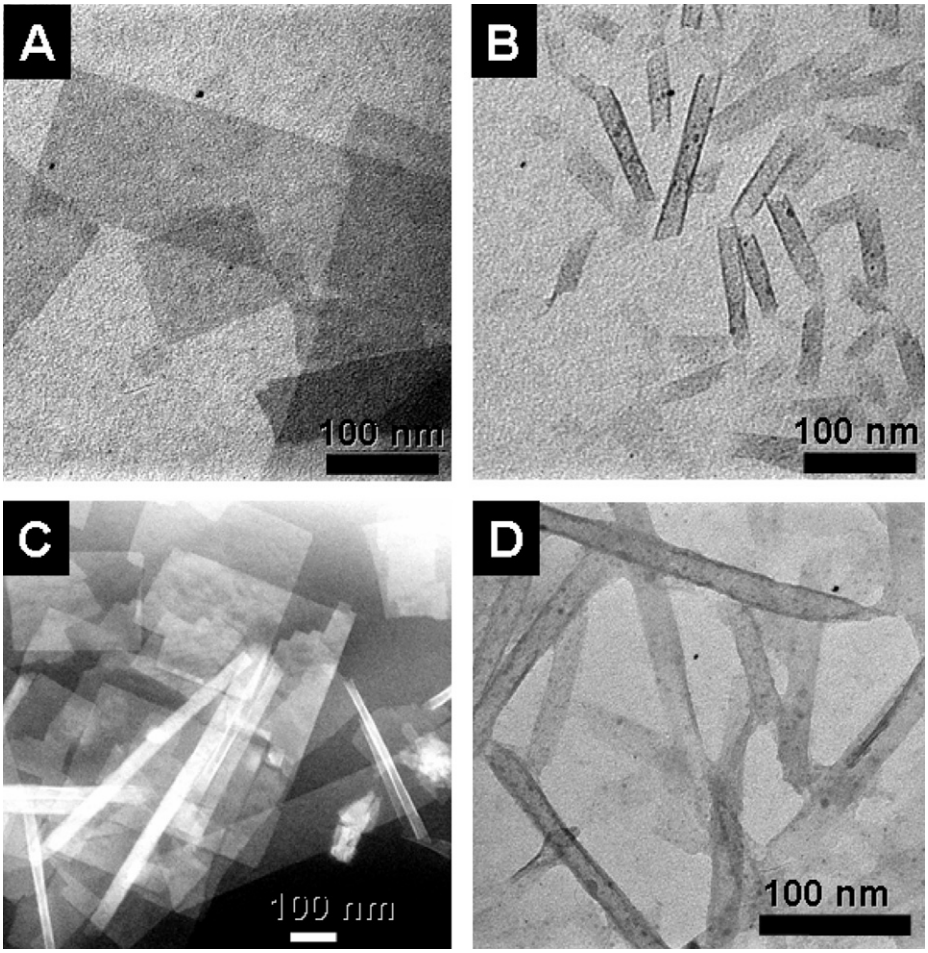

Fig. 2. TEM of (A) PA sheets and of (B) TBA scrolls. (C) STEM of TBA sheets after irradiation in aqueous methanol, and (D) TEM of TBA scrolls after irradiation in water.

on $K_4Nb_6O_{17}$ powders that give an emission maximum at 420 nm [13]. A reexamination of the fluorescence shows that if the emission spectrum is recorded at 77 K the emission peak does indeed occur at 415–420 nm (Supporting information). A strong temperature dependence of the fluorescence is generally observed for indirect semiconductors. For nanosheets and nanoscrolls, the positions of the room temperature emission peaks are similar to $K_4Nb_6O_{17}$, indicating that the electronic structure of the niobate layers is maintained upon exfoliation. In the case of PA sheets, the emission is narrow compared to the other materials. It is possible that the narrowing of the peak is due to a reduction of mid-bandgap defects that are present in $K_4Nb_6O_{17}$, but that disappear upon exfoliation and purification of the sheets.

All materials, especially the exfoliated ones, also exhibit a weak and broad emission peak at 600–800 nm, which can be assigned to radiative recombination of charge carriers trapped in mid-band states [12]. Variations in the shape and position of these peaks reflect structural differences in the NbO layers and in the layer environment as resulting from bending the niobate layers (scrolls versus sheets) and from differences in solvation (PA versus hydronium versus potassium ions).

To determine the effect of the morphology of the niobate layers on the timescale of charge carrier dynamics, femtosecond transient absorption spectroscopy measurements were conducted on PA sheets and TBA scrolls. Both exhibit a broad visible transient absorption (Fig. 4A) that decays according to non-exponential, fluence-dependent dynamics, similar to what has been previously observed for $K_4Nb_6O_{17}$ [15] and $HCa_2Nb_3O_{10}$ nanosheets [12]. Trapped holes exhibit an absorption peak around 450 nm and trapped electrons absorb most strongly around 700 nm. These species decay through electron–hole recombination with approximately second-order kinetics as a result of nongeminate

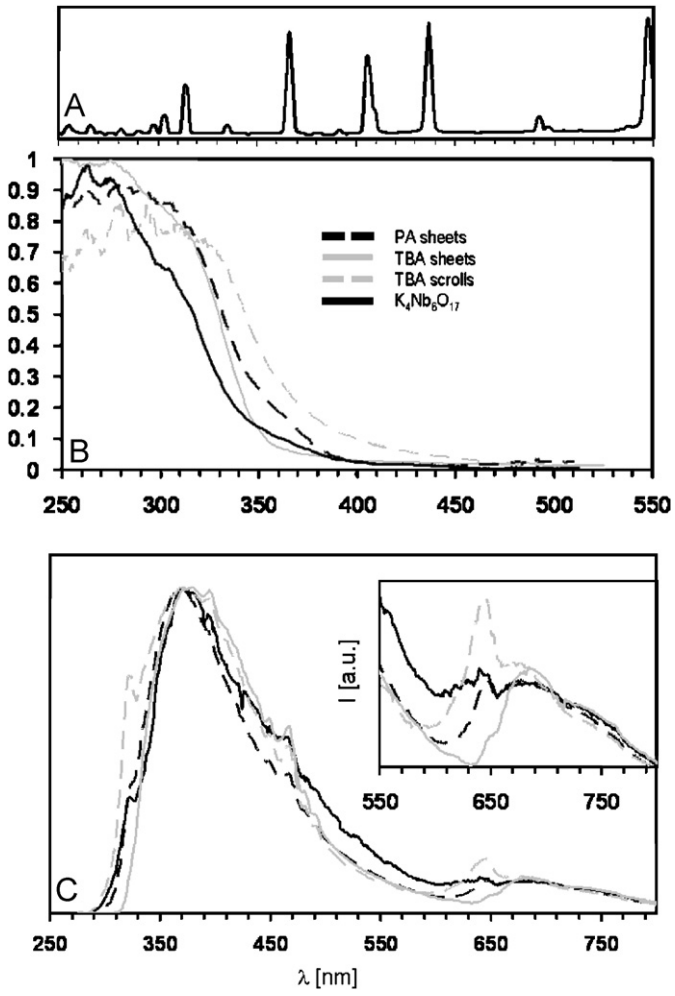

Fig. 3. Optical properties of Hg light source and catalysts. (A) Hg emission spectrum. (B) Diffuse reflectance UV–vis spectra of thin films of the catalysts after drying from aqueous solution. (C) Normalized emission spectra ($\lambda_{ex} = 275$ nm, room temperature) of catalysts dispersed in water. The inset shows magnified region 550–800 nm.

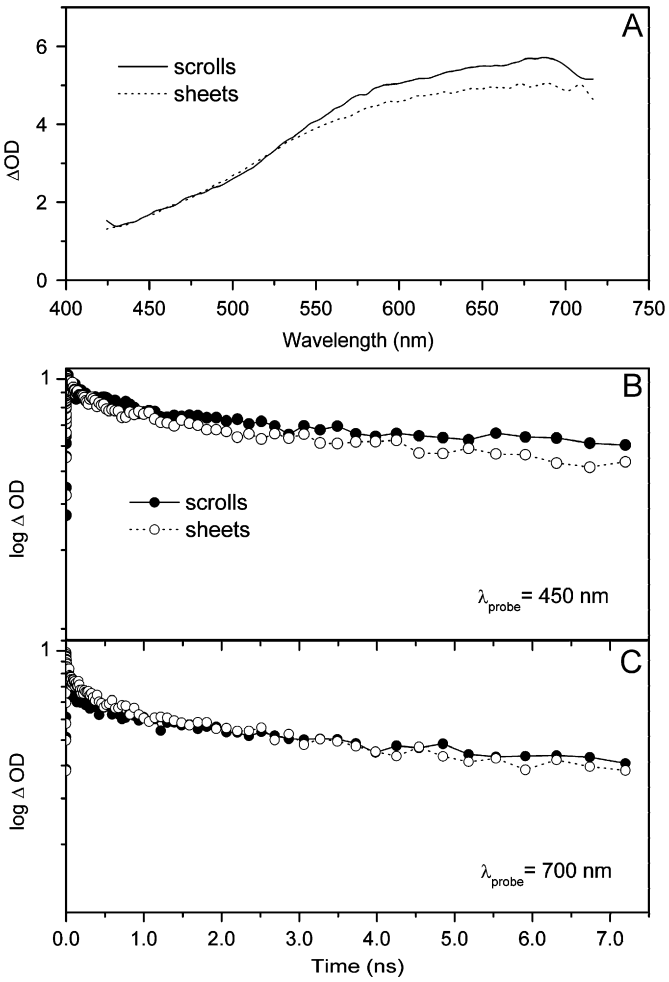

Fig. 4. (A) Transient spectrum 1 ps following 300 nm excitation of PA sheets and TBA scrolls in water. (B and C) Normalized kinetics at 450 and 700 nm.

Table 1
Optical properties

	$K_4Nb_6O_{17}$	PA sheets	TBA sheets	TBA scrolls
Absorption edge	348 nm/3.56 eV	360 nm/3.44 eV	352 nm/3.52 eV	375 nm/3.30 eV
Emission maximum	376 nm/3.29 eV	371 nm/3.34 eV	380 nm/3.26 eV	372 nm/3.33 eV
Emission width at half maximum	143 nm	110 nm	136 nm	134 nm

recombination and higher-order relaxation processes. The initial transient spectra of TBA scrolls and PA sheets exhibit a difference in the absorption at $\lambda > 550$ nm in scrolls (Fig. 4A). The greater absorption of the scrolls can represent either a larger absorption cross-section for trapped electrons as compared to sheets or a larger trapped electron population relative to the population of trapped holes. Analysis of the kinetics at 450 and 700 nm (Fig. 4B and C) supports the latter interpretation, considering that the rate of decay is inversely proportional to carrier population for second-order kinetics. The intrinsic recombination rate of each material cannot be determined without knowledge of the number of excitons generated on an individual sheet or scrolls [12,16]. However, within the uncertainty of exciton density associated with the large size-dispersion of these samples, our measurement indicates that the intrinsic recombination rates in sheets and scrolls are not significantly different.

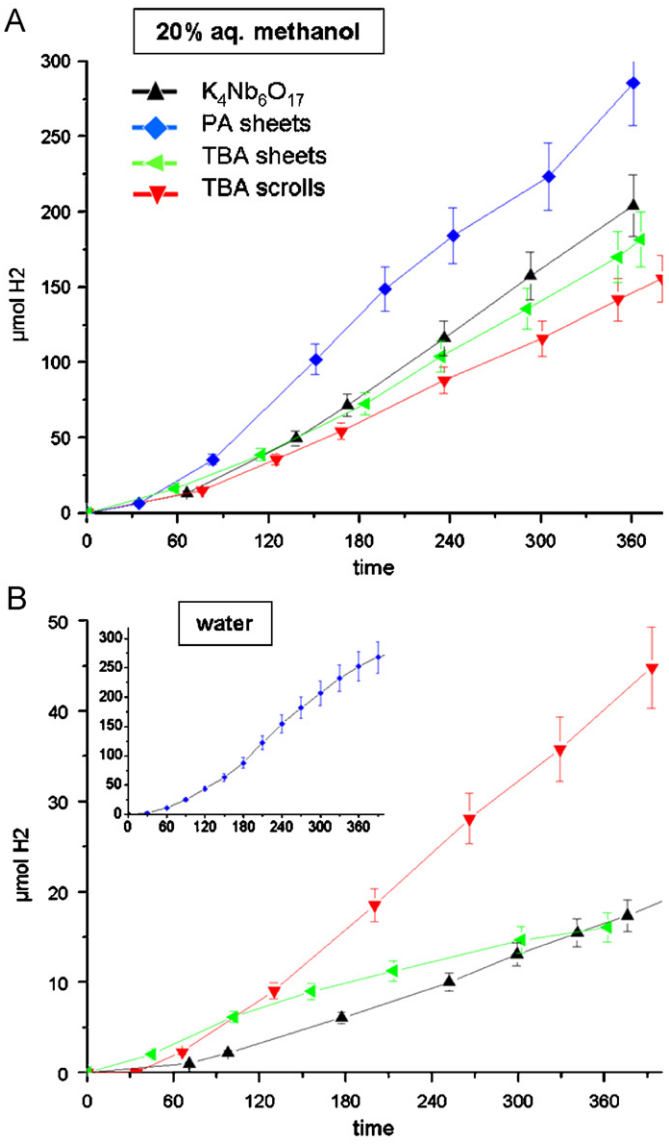

Fig. 5. H_2 evolution data from 20%(vol) aqueous methanol (A) and from water (B). The inset in B shows data for PA sheets.

To determine the effect of morphology on catalytic H_2 evolution from water and aqueous methanol (20%), particle dispersions in the respective media were irradiated simultaneously with four 175 W low-pressure mercury lamps. H_2 evolution curves and selected data are shown in Fig. 5 and Table 2. In aqueous methanol, all materials were found to steadily produce H_2. After 6 h the total evolved amount of H_2 was at least twice the molar amount of the catalysts, proving the catalytic nature of the process. Overall, we find the activity of the nanomaterials to be similar to the parent phase $K_4Nb_6O_{17}$, or slightly higher in the case of PA sheets. In these systems, methanol reduces the niobate in the excited state, which subsequently donates the electron to water [1]. The data show that exfoliation does not increase the activity of the niobate. That agrees with previous evidence for effective methanol penetration into the interlayer space of $K_4Nb_6O_{17}$ [17]. For PA sheets, the slightly higher activity is likely due to the presence of propylamine, which gets oxidized preferentially over methanol. Butylamine has been previously shown to be an effective electron donor under photocatalytic conditions [18,19]. As expected, when PA is substituted with TBA, the activity for H_2 evolution is reduced and becomes comparable to that of $K_4Nb_6O_{17}$.

The involvement of PA in the redox reactions and its oxidation over long irradiation times (>6 h) are further supported by transient absorption experiments of the sheets conducted before and after photolysis (Supporting information). For freshly exfoliated PA sheets, the dynamics observed in both water and aqueous methanol solutions are indistinguishable, suggesting that on the nanosecond timescale methanol cannot compete with PA as a sacrificial donor. However, following photo-oxidation of PA after 6 h of irradiation, the carrier dynamics were found to be sensitive to methanol and sub-nanosecond hole scavenging was observed [12].

From pure water, $K_4Nb_6O_{17}$ and all derived nanomaterials also evolve hydrogen gas under UV irradiation, although at a greatly diminished rate. Only PA sheets have nearly the same activity as observed in aqueous methanol, due to the sacrificial role of the

Table 2
Catalytic activity

	$K_4Nb_6O_{17}$ (100 mg)	PA sheets (100 mg)	TBA sheets (100 mg)	TBA scrolls (100 mg)
20% methanol				
pH before (after) irradiation	10.05 (10.00)	9.00 (7.10)	9.44 (7.71)	10.25 (9.41)
H_2 (µmol) after 6 h	203.6	285.0	178.7	147.6
H_2 rate (µmol/h)	33.9	47.5	29.8	24.6
QE (%)	3.24	4.53	2.84	2.35
Water				
pH before (after) irradiation	10.42 (9.20)	9.32 (6.93)	9.19 (7.19)	9.88 (8.49)
H_2 (µmol) after 6 h	16.6	250.0	16.0	41.0
H_2 rate (µmol/h)	2.8	41.7	2.7	6.8
QE (%)[a]	0.28	3.97	0.25	0.65

Catalyst amount: 100 mg, liquid volume: 75 mL.
[a] QEs based on the photon flux across the full emission spectrum of Hg lamps. Actual QEs are higher, because catalysts only absorb <400 nm.

surface-adsorbed PA. As the PA is consumed, the H_2 rate decreases with time. If PA is replaced with TBA, the activity becomes comparable to TBA scrolls and $K_4Nb_6O_{17}$. For none of the materials could oxygen be detected in the headspace of the reactor. The lack of oxygen evolution has been noted for wide band semiconductors TiO_2 and niobates [5,20–22], and is generally attributed to either incomplete water oxidation leading to surface-bound hydrogen peroxide, or rapid photoreduction and adsorption of oxygen generated by the oxidation of water. We previously observed that for Pt-modified $HCa_2Nb_3O_{10}$ nanosheets the accumulation of water oxidation products on the catalyst surface shuts down H_2 evolution after 9 h [23]. For TBA sheets and TBA scrolls, no significant drop in H_2 evolution rate was observed for 30 h constant irradiation (Supporting information), because water redox reactions are much slower in the absence of Pt cocatalysts. Comparing PA-free catalysts, one finds that the activity of TBA scrolls is nearly twice that of the TBA sheets and $K_4Nb_6O_{17}$.

This enhanced activity could be caused by several factors. First, it could be due to a bandgap reduction resulting from bending of the niobate layers. The reduced bandgap shifts the absorption edge into the visible, enabling better overlap with the 365 nm emission line in the Hg spectrum (Fig. 3A). Second, it could be due to a larger trapped electron population relative to the population of trapped holes, as indicated by the greater absorption in the 500–700 nm region of the transient absorption spectrum. Excess electrons would be expected to promote water reduction. Third, due to their folding, scrolls contain interlayer III that is not present in either $K_4Nb_6O_{17}$ or TBA sheets. This configuration may be advantageous for water reduction.

4. Conclusions

In summary, we have shown that the catalytic activity of $K_4Nb_6O_{17}$ for photochemical H_2 evolution from water and aqueous methanol is preserved in pseudo-molecular fragments of the parent compound. This shows that exciton generation and water redox reactions in these systems are intra-layer processes that do not require the presence of a three-dimensional layer framework as present in the parent material. It also demonstrates that surface area is not the limiting factor in these catalysts. The activities of the nanoscale catalysts are affected by propylammonium, which acts as a sacrificial donor. For scrolls, the observed enhanced activity in water could be either due to the structural features of a new type of interlayer, due to a reduced bandgap from bending, or due to a larger trapped electron population, as suggested by transient absorption spectra. Apart from this, the intrinsic recombination rates in sheets and scrolls are not significantly different.

Acknowledgments

This work was supported by an Energy Innovation Startup Grant of the California Energy Commission (Osterloh), and by DoE grant DE-FG02-03ER46057 (Browning).

Appendix A. Supporting information

Supplementary data associated with this article can be found in the online version at doi:10.1016/j.jssc.2008.06.021.

References

[1] K. Domen, A. Kudo, M. Shibata, A. Tanaka, K. Maruya, T. Onishi, J. Chem. Soc. Chem. Commun. (23) (1986) 1706–1707.
[2] K. Sayama, A. Tanaka, K. Domen, K. Maruya, T. Onishi, Catal. Lett. 4 (3) (1990) 217–222.
[3] H.G. Kim, D.W. Hwang, J. Kim, Y.G. Kim, J.S. Lee, Chem. Commun. (12) (1999) 1077–1078.
[4] K. Sayama, A. Tanaka, K. Domen, K. Maruya, T. Onishi, J. Catal. 124 (2) (1990) 541–547.
[5] S. Tabata, H. Ohnishi, E. Yagasaki, M. Ippommatsu, K. Domen, Catal. Lett. 28 (2–4) (1994) 417–422.
[6] K. Sayama, A. Tanaka, K. Domen, K. Maruya, T. Onishi, J. Phys. Chem. 95 (3) (1991) 1345–1348.
[7] M. Gasperin, M.T. Lebihan, J. Solid State Chem. 43 (3) (1982) 346–353.
[8] K. Domen, in: M. Kaneko, I. Okura (Eds.), Photocatalysis Science and Technology, Springer, New York, 2002, pp. 261–278.
[9] N. Miyamoto, H. Yamamoto, R. Kaito, K. Kuroda, Chem. Commun. (20) (2002) 2378–2379.
[10] G.B. Saupe, C.C. Waraksa, H.-N. Kim, Y.J. Han, D.M. Kaschak, D.M. Skinner, T.E. Mallouk, Chem. Mater. 12 (6) (2000) 1556–1562.
[11] K. Nassau, J.W. Shiever, J.l. Bernstei, J. Electrochem. Soc. 116 (3) (1969) 348–353.
[12] E.C. Carroll, O.C. Compton, D. Madsen, D.S. Larsen, F.E. Osterloh, J. Phys. Chem. C 112 (7) (2008) 2394–2403.
[13] A. Kudo, T. Sakata, J. Phys. Chem. 100 (43) (1996) 17323–17326.
[14] Y.I. Kim, S.J. Atherton, E.S. Brigham, T.E. Mallouk, J. Phys. Chem. 97 (45) (1993) 11802–11810.
[15] A. Furube, T. Shiozawa, A. Ishikawa, A. Wada, K. Domen, C. Hirose, J. Phys. Chem. B 106 (12) (2002) 3065–3072.
[16] G. Rothenberger, J. Moser, M. Gratzel, N. Serpone, D.K. Sharma, J. Am. Chem. Soc. 107 (26) (1985) 8054–8059.
[17] Y. Ebina, A. Tanaka, J.N. Kondo, K. Domen, Chem. Mater. 8 (10) (1996) 2534–2538.
[18] K. Shimizu, Y. Tsuji, T. Hatamachi, K. Toda, T. Kodama, M. Sato, Y. Kitayama, Phys. Chem. Chem. Phys. 6 (5) (2004) 1064–1069.
[19] K. Shimizu, S. Itoh, T. Hatamachi, T. Kodama, M. Sato, K. Toda, Chem. Mater. 17 (20) (2005) 5161–5166.
[20] A. Mills, G. Porter, J. Chem. Soc. Faraday Trans. I 78 (1982) 3659–3669.
[21] K. Sayama, K. Yase, H. Arakawa, K. Asakura, A. Tanaka, K. Domen, T. Onishi, J. Photochem. Photobiol. A 114 (2) (1998) 125–135.
[22] E. Yesodharan, S. Yesodharan, M. Gratzel, Sol. Energy Mater. 10 (3–4) (1984) 287–302.
[23] O.C. Compton, C.H. Mullet, S. Chiang, F.E. Osterloh, J. Phys. Chem. C 112 (15) (2008) 6202–6208.